Article:
Doğan, Ümit, Sarcan, Fahrettin, Hut, Elanur et al. (6 more authors) (2024) Characterization of composition dependence of properties of a MgNiO-based MSM structure. Physica Scripta. 095974. ISSN 0031-8949

https://doi.org/10.1088/1402-4896/ad6e3d

PAPER • OPEN ACCESS

Characterization of composition dependence of properties of a MgNiO-based MSM structure

Physica Scripta

PAPER

Characterization of composition dependence of properties of a MgNiO-based MSM structure

Ümit Doğan[1], Fahrettin Sarcan[1], Elanur Hut[1], Barat Achinuq[2], Ahmad Althumali[3,4], Ibrahim Aldawood[3,5], Adam Kerrigan[2], Vlado K Lazarov[2,3] and Ayşe Erol[1]

[1] Department of Physics, Faculty of Science, Istanbul University, Vezneciler, 34134, Istanbul, Turkey
[2] York-JEOL Nanocentre, University of York, Heslington, York, YO10 5DD, United Kingdom
[3] School of Physics, Engineering and Technology, University of York, Heslington, York, YO10 5DD, United Kingdom
[4] Department of Physics, Faculty of Science, Taif University, PO Box 11099, Taif 21944, Saudi Arabia
[5] Department of Physics, College of Science and Humanities in Al-Kharj, Prince Sattam bin Abdulaziz University, Al-Kharj 11942, Saudi Arabia

E-mail: fahrettin.sarcan@istanbul.edu.tr

OPEN ACCESS

RECEIVED
17 May 2024

REVISED
5 August 2024

ACCEPTED FOR PUBLICATION
12 August 2024

PUBLISHED
22 August 2024

Keywords: MSM, photodetector, MgNiO, metal-semiconductor-metal, UV, MBE, photoconductivity

Supplementary material for this article is available online

Abstract

In this study, the effect of Mg composition on structural and optical properties of $Mg_xNi_{1-x}O$ alloy thin film single crystal semiconductors as well as their implementation into Metal-Semiconductor–Metal (MSM) photodetector are studied. An 850 meV blue-shift of the bandgap is observed from 3.65 eV to 4.50 eV with increasing Mg composition from 0% to 67%. The deep ultraviolet/visible rejection ratio, which is the ratio of photosensitivity at a peak wavelength of 360 nm to that at 450 nm is found to be ∼58 for Mg composition of 67%. Mg rich (%67 Mg) alloy-based photodetector is found to have two orders smaller dark current and have higher spectral response compared to NiO-based one. Spectral responsivities for $Mg_xNi_{1-x}O$ photodetectors are determined as 415 mA W^{-1}, 80 mA W^{-1}, and 5.6 mA W^{-1} for Mg compositions of 67%, 21%, and 0% (reference-NiO), respectively. Furthermore, the detectivity of the photodetectors enhances as Mg composition increases and the highest detectivity of a magnitude of $\sim 10^{11}$ Jones is found for the photodetector with Mg composition of 67%.

Introduction

In recent years, there has been an increasing demand for photodetectors operating in ultraviolet (UV) (< 400 nm), deep UV (DUV) (< 300 nm) and solar-blind (< 280 nm) wavelength regions with high sensitivity and low noise. DUV photodetectors play a very important role in the fields of flame sensors, chemical-biological sensors, ozone layer monitoring, missile warning systems, short-range secured communications, and space technology. There are several potential semiconductors for DUV photodetectors, such as SiC [1], $Al_xGa_{1-x}N$ [2], Ga_2O_3 [3], and $Mg_xZn_{1-x}O$ [4]. In recent studies, $Mg_xNi_{1-x}O$ has attracted attention beyond these conventional materials thanks to better matched structural properties of its constituent compounds, MgO and NiO [5–11]. Both MgO (4.212 Å) and NiO (4.177 Å) have face centered cubic (rock salt) structure, with only a 0.8% lattice mismatch [12]. Both NiO and MgO are direct bandgap semiconductors with bandgaps of 3.7 eV and 7.8 eV at room temperature, respectively [13, 14]. Alloying these compounds gives a great flexibility to tune the bandgap of the alloy to being within the DUV region, depending on the alloy composition of Mg in $Mg_xNi_{1-x}O$, from 159 nm ($x = 1$) to 365 nm for ($x = 0$) [6, 8].

So far, there have been few reported studies on $Mg_xNi_{1-x}O$ thin films and $Mg_xNi_{1-x}O$-based photodetectors. Kwon *et al* reported on the growth of $Mg_xNi_{1-x}O$ (x = 0.049) thin films using the radio frequency (RF) magnetron sputtering method [15]. In their study, they observed a blue shift from 3.75 eV to 3.95 eV in the bandgap of thin films with increasing RF power of Mg source [15]. Zhao *et al* reported the structural and optical properties of electron beam evaporation deposited $Mg_xNi_{1-x}O$ thin films with 3 different Mg compositions

(x = 0.2, 0.5, 0.8) and focused on the optical and electrical properties of $Mg_xNi_{1-x}O$-based photodetectors at only a single Mg composition (x = 0.2) [9]. They reported that $Mg_{0.2}Ni_{0.8}O$ (x = 0.2)-based photodetector has a dark current of 70 nA at 5 V bias voltage and a responsivity of 145 μA W^{-1} at 320 nm, with a cut-off wavelength of 340 nm [9]. Nishitani *et al* reported the fabrication of a photodetector based on $Mg_xNi_{1-x}O$ (x = 0.48) thin film deposited by RF magnetron sputtering method using a Ni-Mg composite target [16]. They achieved a 7 μA W^{-1} maximum responsivity at 292 nm [16]. Guo *et al* studied the effects of rapid thermal annealing on both the structural and optical properties of $Ni_{1-x}Mg_xO$-based metal-semiconductor–metal (MSM) UV photodetectors grown by pulsed laser deposition (mole content of Mg is around 20%). They reported a 12 meV bandgap blue-shift from 3.78 eV to 3.90 eV for as-deposited to annealing temperature 1000 °C) and 15 times smaller dark current on annealed thin films at 1000 °C compared to as-grown thin films [17]. Mares *et al* for the first time in the literature, grew a $Ni_xMg_{1-x}O$ thin film (4,38 eV for $x = 0.54$) using Molecular Beam Epitaxy (MBE), with the dark current values, rise and fall times of $Mg_xNi_{1-x}O$-based photodetector of < 25 nA, 0.59 s and 7.10 s, respectively [18]. Recently, we have studied $Mg_xNi_{1-x}O$-based photodetector ($x = 0.67$), which was grown by MBE, and have found the spectral responsivity of 415 mA W^{-1} and the dark current of 3.7×10^{-11} A, at 10 V bias voltage [5]. To the best our knowledge, the effect of alloy composition on the performance of $Mg_xNi_{1-x}O$-based photodetectors has not been studied.

In this study, we study composition dependence of structural and optical properties of $Mg_xNi_{1-x}O$ thin films grown by the MBE with different Mg compositions (0, 21 and 67%). Furthermore, for the first time we report alloy composition dependence of the performance of $Mg_xNi_{1-x}O$-based photodetectors grown by MBE

Experimental methods

$Mg_xNi_{1-x}O$ thin films, with Mg compositions of 0, 21 and 67% were epitaxially grown on (111)-oriented $SrTiO_3$ (STO) substrates by MBE Before the growth, the substrates underwent a sequential cleaning procedure, starting with acetone, then followed by isopropanol and deionized water for a period of 10 min each in an ultrasonic bath. The substrates were then annealed at 1100 °C for an hour under atmospheric pressure. All films were deposited for an hour under the following conditions: Ni effusion cell temperature of 1300 °C a substrate temperature of 300 °C and an oxygen partial pressure of 5×10^{-6} mbar. The Mg effusion cell was operated simultaneously with the Ni effusion cell at temperatures of 270 °C and 320 °C. Elemental composition of the grown thin films and their homogeneity have been measured using Energy Dispersive X-Ray Spectroscopy (EDS). The crystal structure of the films was determined by x-ray diffraction (XRD) with $2\theta - \omega$ scan mode, using Rigaku SmartLab with Cu K_α radiation ($\lambda = 1.5418$ Å). Transmission electron microscopy (TEM) measurements were performed on a JEOL 2100+ TEM at the York-JEOL Nanocentre. The specimen preparation for TEM was done using a focused ion beam FEI Nova 200. Surface morphology characterization of the films was carried out by Atomic Force Microscopy (AFM) (Park System, XE-Series). Non-contact mode and NSC 15-type cantilever were utilized in the AFM measurements. Following structural characterization, thin films were fabricated to have contacts in interdigital transducer (IDT) geometry for electrical and electro-optical characterizations. The IDT electrode structures were defined on the films using the conventional photolithography methods. First, the samples were rinsed in acetone and then isopropyl alcohol for 5 min and dried with pure nitrogen (99.999%) gas. After the cleaning procedure, the samples were first prebaked at 110 °C for 60 s. After this procedure, the samples were spin-coated with AZ5214 positive photoresist at 6000 rpm to be 1.4 μm in thickness using a spin coater (SPS SPIN 150). After spin-coated procedure, the baking process was carried out again at 110 °C for 30 s to remove the water in the photoresist. Subsequently, the exposure process to define the IDT pattern was performed using a mask aligner (SUSS MJB4 Mask Aligner) with 405 nm LED (28.8 mW cm^{-2}) and 50 s exposure time. Then development of the IDT pattern was carried out using an AZ400K developer until the IDT geometry appeared on the sample surface. A 10 nm Cr as adhesive layer and 100 nm Au (purity: 99.999%) were coated on the sample using a thermal evaporator (VAKSIS Twin Chamber Thermal Evaporator). The areas on the samples protected from Au coating via photoresist was removed with rinsing the samples in acetone. The samples were stuck on ceramic holders using Ge varnish and 25 μm diameter gold wires were wedge-bonded from IDT to samples holder's gold pads to conduct the electrical and electro-optical measurements. The length of IDT fingers is 450 μm, and both the width and interspacing of the interdigitated electrodes are 20 μm. Spectral photoconductivity measurements were carried out using a free space system equipped with a 450 W Xenon lamp, a lock-in amplifier (SRS, SR-830) and a 0.5 m monochromator (Acton, SP2500i). The current–voltage (I-V) characteristics of the samples were measured with a source/meter unit (Agilent B2902A). Spectral response measurements were carried out by a Xenon lamp and an electronic shutter. Power density of Xenon lamp was kept at about 16 mW cm^{-2} during the measurements. Response values were determined by calculating the time at which the intensity reached 90% and 10% of the maximum photocurrent measurements.

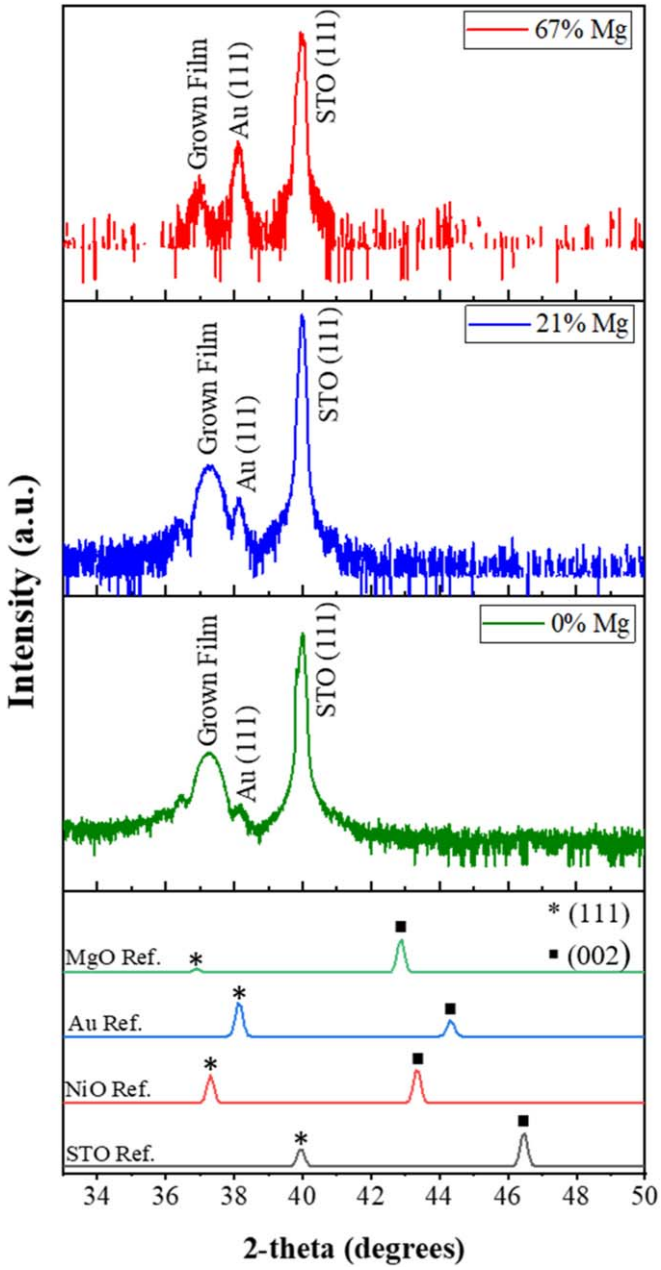

Figure 1. X-ray diffraction patterns of $Mg_xNi_{1-x}O$ thin films for Mg compositions of 0, 21 and 67%. Reference file for substrate, Au, as well as NiO and MgO are also shown for comparison to experimental XRD results.

Result and discussion

Figure 1 shows the representation of a normalized intensity x-ray diffraction patterns of $Mg_xNi_{1-x}O$ with varying Mg composition (0, 21 and 67%), which was measured after the IDT electrode fabrication on the samples. All films have a peak at 40°, which belongs to the (111) plane of STO perovskite crystal structure (ICSD code no. 37464), and another peak at 38.2° corresponding to the (111) plane of Au face centered cubic structure (ICSD code no. 41690), which is the material used for the IDT electrode fabrication. The $Mg_xNi_{1-x}O$, with 0% and 0.21% Mg composition films, exhibit a diffraction peak at 37.3°, which belongs to (111) plane of NiO rock-salt cubic crystal structure (ICSD code no. 112324). For the $Mg_xNi_{1-x}O$, with 67% Mg composition film, as expected the (111) peak has been shifted to lower 2 theta values i.e. 36.9°, reflecting that grown film is dominantly MgO (111) (ICSD code no. 52087). Since Ni and Mg have the same valency, and very similar ionic radii of, 0.69 Å and 0.72 Å, respectively [19], MgO and NiO form continuous solid solution for any concentration of Mg(Ni) [20].

Furter structural studies by TEM show are fully consistent with XRD results confirm the epitaxial growth of the films with the substrate given by following crystallographic relationship: $Mg_xNi_{1-x}O$ (111) ‖ $SrTiO_3$(111) and $Mg_xNi_{1-x}O$ (1–10) ‖ $SrTiO_3$(1–10). Figure 2(a) shows a bright-field image at low magnification of the grown NiO

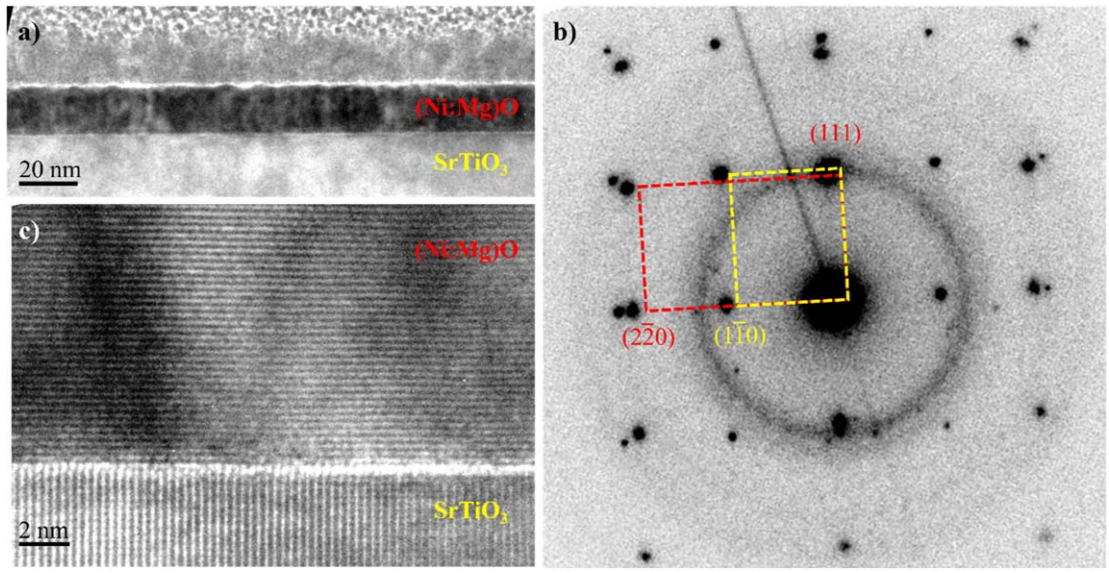

Figure 2. Cross-sectional of NiO (111) / STO (111). (a) Bright field TEM showing the 20 nm thick film, (b) selected area diffraction from NiO film and substrate showing the epitaxy and single crystal structure of the grown NiO film, (c) HRTEM form the interface between the substrate $SrTiO_3$ and the NiO film showing the (111) planes for the film parallel to the interface.

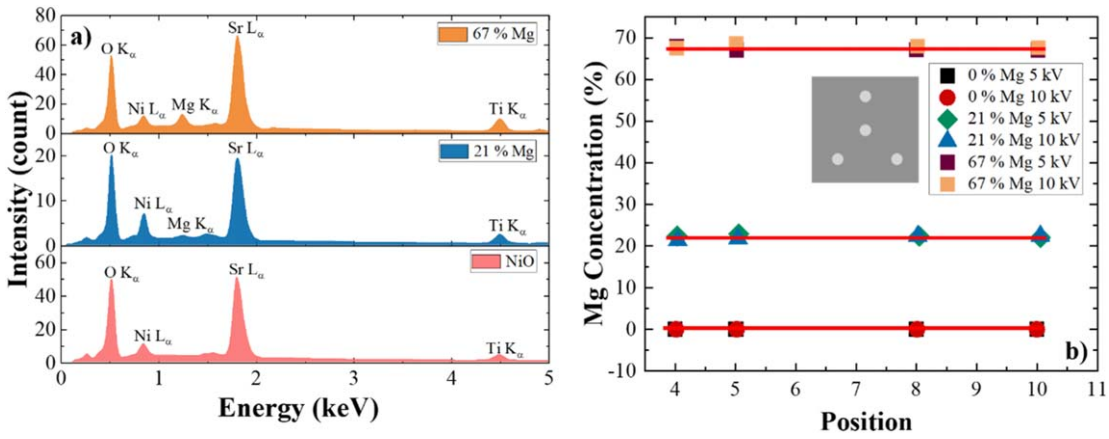

Figure 3. (a) EDS results of $Mg_xNi_{1-x}O$ thin films. (b) Mapping of elemental composition of Mg on the sample.

film, with atomic (111) planes parallel to the interface, as clearly outlined by the HRTEM image, figure 2(c). The single crystal nature, as well as the epitaxy of the grown film, is shown by the selected area diffraction from the substrate and the film shown in figure 2(b). Further alloying by Mg does not change crystallinity of the film, as seen by XRD in figure 1, and directly by HRTEM image in the supplementary figure 1.

SEM-EDS measurements were caried out to determine the elemental composition of $Mg_xNi_{1-x}O$ thin films as shown in figure 3(a). EDS measurements were carried out from various positions as well to determine homogeneity of Mg as shown in inset of figure 3(b). In figure 3(b), the Mg composition measured at four different positions of the sample shows that the Mg distribution in the grown films is homogeneous.

It has been reported that as surface roughness increases, surface scattering mechanisms may effect optical processes such as absorption, reflection and transmission of thin films. Furthermore, small surface roughness can generate a homogeneous electric field across the entire device, thereby reducing the direct tunneling current and potentially enhancing the rectification ratio of the device [21–24]. It has been reported that bandgap, absorption mechanisms and electric field distribution are affected by surface roughness which influence photodetector performance [21–23, 25, 26]. Therefore, AFM measurement was carried out on the samples. The composition dependence of surface roughness of the grown thin films is presented in figure 4. The surface roughness of the thin films was determined to be 1.5 ± 0.5 nm, 3.0 ± 0.5 nm, and 3.5 ± 0.5 nm for Mg

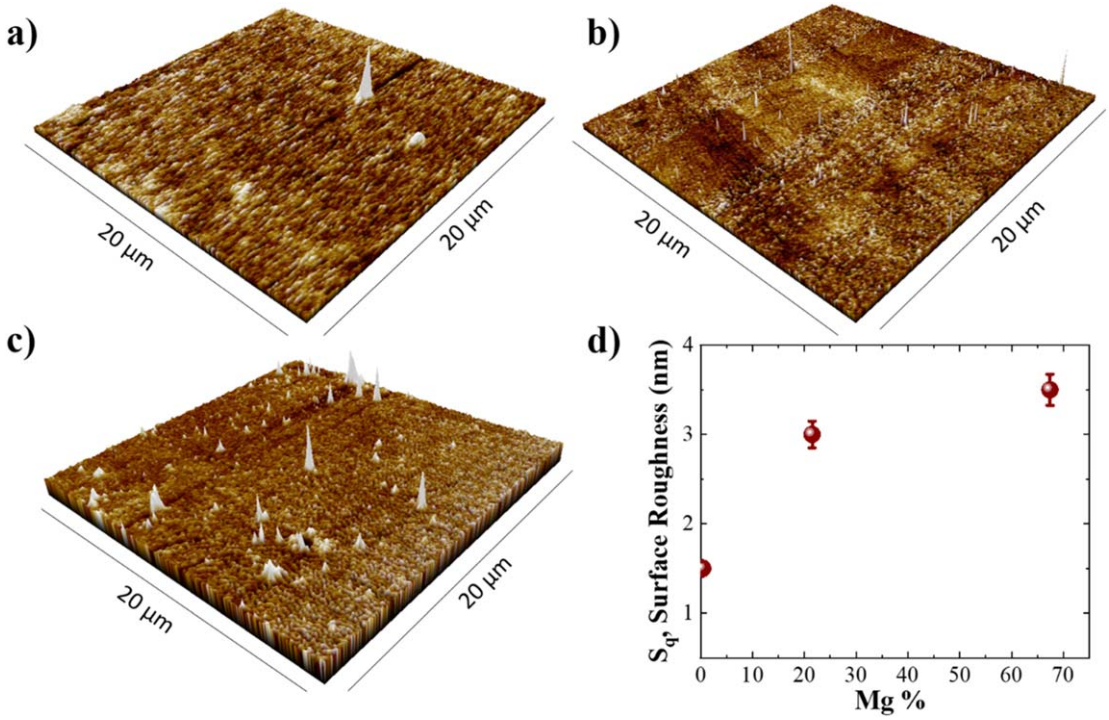

Figure 4. AFM images of the $Mg_xNi_{1-x}O$ thin films for Mg compositions of (a) 0%, (b) 21%, (c) 67% and (d) composition dependence of surface roughness of $Mg_xNi_{1-x}O$.

compositions 0, 21 and 67%, respectively, revealing that the surface roughness slightly increases with increasing Mg composition.

To investigate the composition dependence of bandgap of the alloy, spectral photoconductivity measurements were carried out using IDT electrode configuration defined on the sample surface via conventional photolithography techniques as explained above. The IDT structure was patterned with a length of IDT fingers is 450 μm, where both the width and interspacing of the interdigitated electrodes are 20 μm. This electrode configuration on $Mg_xNi_{1-x}O$ thin films is also e structure of the fabricated MSM photodetectors (figure 5(a)). Energy band diagram of Au/$Mg_xNi_{1-x}O$ depending on alloy composition is shown in figure 5(b). The bandgap of NiO is ∼3.7 eV [14]. The work functions of NiO and Au are 6.7 eV and 5.4 eV, respectively [27, 28], and NiO is a well-known p-type material in nature [11, 29, 30]. Alloying NiO with Mg blue-shifts the bandgap of $Mg_xNi_{1-x}O$ according to Vegard's law as discussed below. Au/NiO and Au/$Mg_xNi_{1-x}O$ forms Schottky contact. The IDT contact pattern define MSM structure on the surface of the thin film. MSM structured photodetectors are basically composed of two Schottky contacts [31–34]. When no bias voltage is applied to the contacts, the band structure of the photodetector is as shown in figure 5(c), but when a bias voltage is applied to the contacts, one side is forward biased while the other side is reverse biased. When a bias voltage is applied between the contacts, since one contact is forward biased and the other is reverse biased, the depletion region on the reverse biased side expands. When the bias voltage is increased and reaches a certain level, the width of the depletion region increases and reaches the other contact. In this case, the band bending disappears, and the bands take on a tilted flat structure leading to Ohmic behavior in I-V curves of MSM structures. When light is incident on the photodetector under this bias voltage, electron–hole pairs are generated. The generated photocarriers move towards the contacts and are collected, resulting in a photocurrent (I_{ph}). The state of the bands under bias voltage is shown in figure 5(d).

Responsivity (R) and detectivity (D^*) of the photodetectors were calculated using [35–37]:

$$R = \frac{I_p - I_d}{P.S} \tag{1}$$

$$D^* = \frac{R}{\sqrt{2eI_d/S}} \tag{2}$$

where I_p is total current under illumination and I_d is dark current (dark currents used $I_d = 5.5 \times 10^{-9}$ A, 4.1×10^{-10} and 3.7×10^{-11} for Mg compositions 0, 21 and 67%, respectively), P is the power density of light source ($P_{Xe} = 16$ mW cm^{-2}), S is active area of the photodetectors ($S = 0.192$ mm^2), e is the electron charge (1.6×10^{-19} C). Responsivity values of the photodetectors are found to be 415 mA W^{-1} (67% Mg), 80 mA W^{-1}

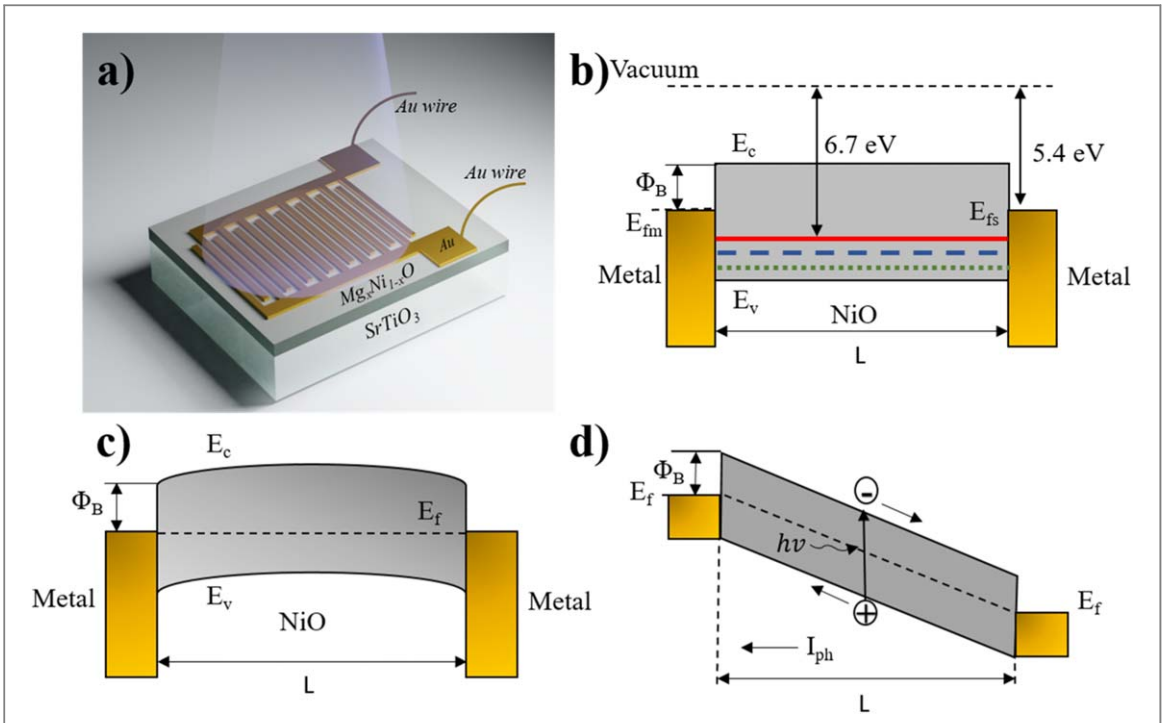

Figure 5. (a) Schematic illustration of the fabricated $Mg_xNi_{1-x}O$ photodetector, (b) band line-up of Au/$Mg_xNi_{1-x}O$ for 0% (solid red line), 21% (dashed blue line) and 67% (dotted green line) Mg compositions. Also shown, an energy band diagram of a p-type NiO-based ideal MSM photodetector (c) at equilibrium and (d) under bias voltage.

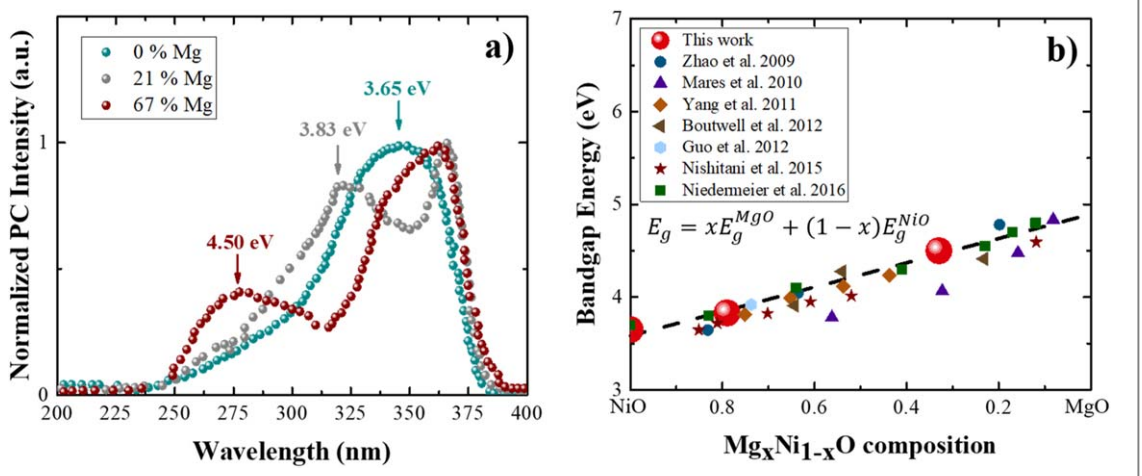

Figure 6. (a) Spectral photoconductivity of the $Mg_xNi_{1-x}O$ photodetectors without applied bias and (b) Composition dependence of the bandgap of $Mg_xNi_{1-x}O$. Red circles indicate the results obtained in this study, and literature values are taken from [6, 9, 13, 14, 16, 18, 38, 39].

(21% Mg), 5.6 mA W^{-1} (0% Mg) at a bias voltage of 10 V under illumination by a 320 nm line of Xenon. The detectivities are 1.98×10^{12} Jones, 1.14×10^{11} Jones, 2.19×10^{9} Jones for 67%, 21%, 0% Mg compositions, respectively. Due to the decrease in dark current depending on the Mg composition, the photosensitivity of the photodetectors has increased four orders.

Figure 6(a) shows the spectral photoconductivity of the samples, which also represents the spectral response of the $Mg_xNi_{1-x}O$-based MSM photodetectors. We have determined the composition dependence of the band gap using spectral photoconductivity measurement, as reported elsewhere [11, 31, 32]. A blue-shift of 850 meV from 3.65 eV (Mg 0%) to 4.50 eV (Mg 67%) is observed with the increasing of Mg composition.

The bandgap of alloys is calculated by Vegard's law

$$E_g(Mg_xNi_{1-x}O) = xE_g(MgO) + (1-x)E_g(NiO) \quad (3)$$

where E_g ($Mg_xNi_{1-x}O$) is the bandgap of alloy semiconductor, E_g(MgO) and E_g(NiO) are the bandgap of MgO and NiO, respectively.

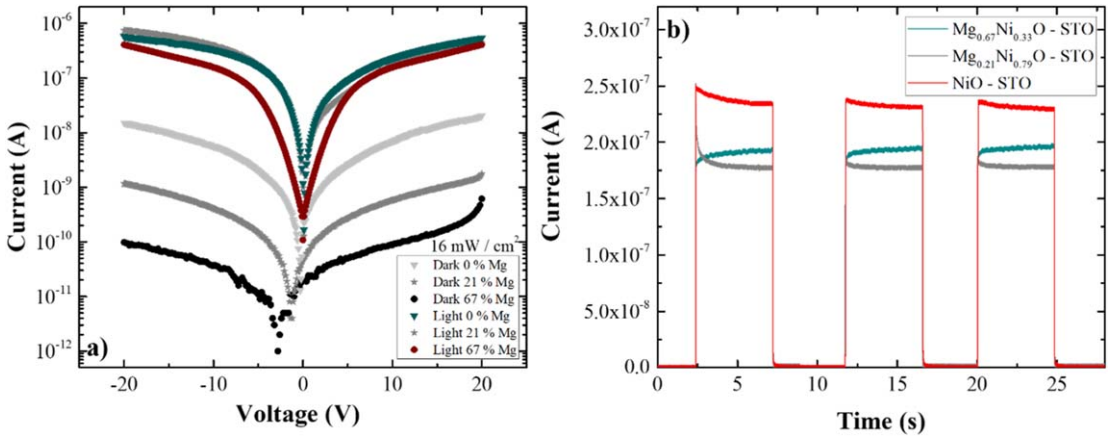

Figure 7. (a) Dark and illuminated I-V characteristics of $Mg_xNi_{1-x}O$ photodetectors with various Mg compositions (0, 21 and 67%). (b) The time-dependent photocurrent of $Mg_xNi_{1-x}O$ photodetectors.

The bandgap of STO is about 3.35 eV which corresponds to 370 nm [5, 9], and the bandgap of NiO is about 3.65 eV (340 nm). With increasing Mg concentration, the bandgap of MgNiO blue-shifts, making possible to observe well-resolved peaks. The bandgap of $Mg_xNi_{1-x}O$ films were found to be 3.65 eV, 3.83 eV, and 4.50 eV depending on the Mg compositions of 0, 21 and 67%, respectively, without consideration of the bowing parameter (figure 6). These values well-match with the spectral PC results. When the composition dependence of the bandgap values is compared with the current literature values as shown in figure 6(b), the bandgaps of the $Mg_xNi_{1-x}O$-STO are in the range where Vegard's law is valid.

Figure 7(a) shows the room temperature I-V characteristics of $Mg_xNi_{1-x}O$ photodetectors at dark and under uniform illumination of the Xenon lamp at 450 W. It is found that the dark current of the photodetectors 100-fold decreased with increasing Mg composition compared to that of NiO based photodetector (table 1).

Figure 7(b) shows time-dependent photocurrent of $Mg_xNi_{1-x}O$ thin films. The experiments were carried out using a 450 W Xenon lamp as an excitation source under a bias voltage of 10 V. As a result of taking the measurements without dispersing the Xe light source, the photocurrent of NiO is higher compared to $Mg_xNi_{1-x}O$. Since the light intensity of Xe lamp in the cut-off wavelength of NiO ~ 340 nm is much higher than the light intensity in the DUV region where $Mg_xNi_{1-x}O$ cut-off wavelength lies in, the photocurrent value is observed to be higher for NiO in the time-dependent current measurements. While the fall and rise times of $Mg_xNi_{1-x}O$ photodetectors are comparable, it was observed that photodetector parameters are improved with Mg incorporation. Furthermore, in contrast to the findings in literature, in this study we have observed shorter rise (10.7×10^{-3} s) and fall times (8.6×10^{-3} s), which can be attributed to single crystal nature of the active layer (s), NiO and $Mg_xNi_{1-x}O$. Comparison of $Mg_xNi_{1-x}O$ photodetectors parameters with the reported ones are tabulated in table 1. It is worth noting that photodetector parameters in this study are superior to the reported ones in the current literature.

Conclusions

In conclusion, this study includes the growth and characterization of epitaxial $Mg_xNi_{1-x}O$ photodetectors on STO (111) and their subsequent application in photoconductive deep ultraviolet (DUV) detectors, depending on the alloy composition. Photodetectors with different alloy compositions (0, 21, and 67%) were fabricated through the deposition of interdigitated Au/Cr contacts and were comprehensively characterized regarding their time dependence response, spectral response as well as the voltage-dependent responsivity and dark current. The XRD measurements show that NiO and $Mg_xNi_{1-x}O$ films were grown along the [111] direction, with (111) planes parallel to the substrate. The surface roughness of the grown films correlates with Mg composition within the $Mg_xNi_{1-x}O$ films, initially leading to larger increase. EDS measurement results taken at different accelerating voltages and positions has confirmed the homogeneous composition of the grown $Mg_xNi_{1-x}O$ thin films. Electrical measurements indicate that the dark current values of $Mg_xNi_{1-x}O$ photodetectors decrease with increase of Mg composition, resulting in a 100-fold increase in photosensitivity. As Mg composition increases the photoresponsivity values changes 415 mA W^{-1}, 80 mA W^{-1}, and 5.6 mA W^{-1}. Spectral response measurements have indicated that the bandgap of $Mg_xNi_{1-x}O$ photodetectors blueshifts by approximately 850 meV, depending on the alloy composition. Time-dependent current measurements demonstrated that the rise and fall times of the produced $Mg_xNi_{1-x}O$ photodetectors were less than 10 ms.

Table 1. Photodetector parameters of $Mg_xNi_{1-x}O$ photodetectors in this work compared with reported ones.

Samples	Growth method	Bias (V)	Dark current (A)	Photo sensitivity (I_{photo}/I_{dark}) ratio	Responsivity (AW^{-1})	Detectivity (jones) ($mHz^{1/2}W^{-1}$)	Rise time (s)	Fall time (s)	References
$Mg_{0.67}Ni_{0.33}O$-$SrTiO_3$	MBE	10	3.7×10^{-11}	41.34×10^2	4.15×10^{-1}	1.355×10^{11}	10.7×10^{-3}	8.6×10^{-3}	This Work
$Mg_{0.21}Ni_{0.79}O$-$SrTiO_3$	MBE	10	4.1×10^{-10}	8.08×10^2	8.0×10^{-2}	7.85×10^9	20.97×10^{-3}	7.10×10^{-3}	This Work
NiO-$SrTiO_3$	MBE	10	5.5×10^{-9}	37.85	5.6×10^{-3}	1.5×10^8	7.18×10^{-3}	6.20×10^{-3}	This Work
$Mg_{0.2}Ni_{0.8}O$-Quartz	E-Beam Evaporation	5	70×10^{-9}	—	1.43×10^{-4}	—	—	—	[9]
$Ni_{0.54}Mg_{0.46}O$-MgO	MBE	5	25×10^{-9}	—	1.2×10^{-2}	—	0.59	7.10	[18]
$Mg_{0.20}Ni_{0.80}O$-Quartz	Pulsed Laser Deposition	5	19.6×10^{-9}	—	—	—	—	—	[17]
$Ni_{0.52}Mg_{0.48}O$-Quartz	RF Magnetron Sputtering	—	—	—	6.5×10^{-9}	—	—	—	[16]

Furthermore, the detectivity value, which demonstrates the detection capability of the photodetectors, increases with increasing Mg composition to the order of 10^{11} Jones depending on the Mg composition. The observed low dark current value and fast rise and fall times indicate that $Mg_xNi_{1-x}O$-based-MSM photodetectors are promising to be used in DUV region of electromagnetic spectrum.

Acknowledgments

This work was supported by the Scientific Research Projects Coordination Unit of İstanbul University (Project Number: FDK-2023-39764) and The Scientific and Technological Research Council of Turkey (TUBITAK) (Project Number: 118C117).

Data availability statement

All data that support the findings of this study are included within the article (and any supplementary files).

ORCID iDs

Ümit Doğan https://orcid.org/0000-0002-7317-8497
Fahrettin Sarcan https://orcid.org/0000-0002-8860-4321
Ahmad Althumali https://orcid.org/0000-0001-7679-4028
Ayşe Erol https://orcid.org/0000-0003-4196-1791

References

[1] Li M Q, Yang N, Wang G G, Zhang H Y and Han J C 2019 Highly preferred orientation of Ga_2O_3 films sputtered on SiC substrates for deep UV photodetector application *Appl. Surf. Sci.* **471** 694–702
[2] Cai Q *et al* 2021 Progress on AlGaN-based solar-blind ultraviolet photodetectors and focal plane arrays *Light: Sci. Appl.* Nature **10** 94
[3] Qin Y *et al* 2020 Metal–semiconductor–metal ε-Ga_2O_3 solar-blind Photodetectors with a record-high responsivity rejection ratio and their gain mechanism *ACS Photonics* **7** 812–20
[4] Tsay C Y, Chen S T and Fan M T 2019 Solution-processed Mg-substituted ZnO thin films for metal-semiconductor-metal visible-blind photodetectors *Coatings* **9** 277
[5] Sarcan F, Orchard S, Kuerbanjiang B, Skeparovski A, Lazarov V K and Erol A 2020 Ultraviolet photodetector based on $Mg_{0.67}Ni_{0.33}O$ thin film on $SrTiO_3$ *Phys. Status Solidi - Rapid Res. Lett.* **14** 2000175
[6] Yang Z G, Zhu L P, Guo Y M, Ye Z Z and Zhao B H 2011 Preparation and band-gap modulation in MgxNi1 - XO thin films as a function of Mg contents *Thin Solid Films* **519** 5174–7
[7] Qammar M, Malik Z, Malik F, Baig T and Chaudhary A J 2019 Antibacterial activity of Mg1-xNixO(x = 0.5) nano-solid solution; experimental and computational approach *J. Mol. Struct. Elsevier B.V.* **1179** 347–53
[8] Li G, Zhang J and Hou X 2014 High-responsivity UV detectors based on MgNiO films grown by magnetron sputtering *Epl* **106** 38002
[9] Zhao Y *et al* 2009 MgNiO-based metal–semiconductor–metal ultraviolet photodetector *J. Phys. D: Appl. Phys.* **42** 92007
[10] Xie W *et al* 2017 The effect of sputtering gas pressure on the structure and optical properties of MgNiO films grown by radio frequency magnetron sputtering *Appl. Surf. Sci.* **405** 152–6
[11] Sarcan F *et al* 2023 A novel NiO-based p-i-n ultraviolet photodiode *J. Alloys Compd.* **934** 167806
[12] Kuzmin A and Mironova N 1998 Composition dependence of the lattice parameter in NicMg1-cO solid solutions *J. Phys. Condens. Matter* **10** 7937–44
[13] Roessler D M and Walker W C 1967 Electronic spectrum and ultraviolet optical properties of crystalline MgO *Phys. Rev.* APS. **159** 733
[14] Niedermeier C A, Råsander M, Rhode S, Kachkanov V, Zou B, Alford N and Moram M A 2016 Band gap bowing in Ni x Mg 1-x O *Sci. Rep.* **6** 31230
[15] Kwon Y H, Chun S H and Cho H K 2013 Controllable band-gap engineering of the ternary MgxNi1 − xO thin films deposited by radio frequency magnetron sputtering for deep ultra-violet optical devices *Thin Solid Films* **529** 417–20
[16] Nishitani H *et al* 2015 Band gap tuning of Ni1 − xMgxO films by radio-frequency sputter deposition for deep-ultraviolet photodetectors *Appl. Phys. Express* **8** 105801
[17] Guo Y *et al* 2014 Enhanced performance of NiMgO-based ultraviolet photodetector by rapid thermal annealing *Thin Solid Films* **558** 311–4
[18] Mares J W, Boutwell R C, Wei M, Scheurer A and Schoenfeld W V 2010 Deep-ultraviolet photodetectors from epitaxially grown Nix Mg1-x O *Appl. Phys. Lett.* **97** 161113
[19] Chen Y C, Wang Y N and Hsu C H 2012 Enhancement microwave dielectric properties of Mg_2SnO_4 ceramics by substituting Mg^{2+} with Ni 2+ *Mater. Chem. Phys.* **133** 829–33
[20] Kerrigan A, Pande K, Pingstone D, Cavill S A, Gajdardziska-josifovska M, McKenna K P, Weinert M and Lazarov V K 2022 Nano-faceted stabilization of polar-oxide thin films: The case of MgO (111) and NiO (111) surfaces. *Appl. Surf. Sci.* **596** 153490
[21] Bender M *et al* 2003 Highly sensitive ZnO ozone detectors at room temperature *Jpn. J. Appl. Phys.* **42** L435
[22] Marnadu R, Chandrasekaran J, Maruthamuthu S, Balasubramani V, Vivek P and Suresh R 2019 Ultra-high photoresponse with superiorly sensitive metal-insulator-semiconductor (MIS) structured diodes for UV photodetector application *Appl. Surf. Sci.* **480** 308–22
[23] Shewale P S, Lee N K, Lee S H and Yu Y S 2015 Physical and UV photodetection properties of pulsed laser deposited Mg0.05Zn0.95O thin films: effect of oxygen pressure *J. Alloys Compd.* **640** 525–33

[24] Sarcan F, Wang Y, Krauss T F, Erucar T and Erol A 2020 Dilute nitride resonant-cavity light emitting diode *Opt. Laser Technol.* **122** 105888
[25] Balkan N, Erol A, Sarcan F, Al-Ghuraibawi L F F and Nordin M S 2015 Dilute nitride resonant cavity enhanced photodetector with internal gain for the $\lambda \sim 1.3$ μm optical communications window *Superlattices Microstruct.* **86** 467–71
[26] Sarcan F, Nutku F, Nordin M S, Vickers A J and Erol A 2018 A study on the voltage-dependent response of a GaInNAs-based pin photodetector with a quasi-cavity *Semicond. Sci. Technol.* **33** 114006
[27] Greiner M T, Helander M G, Wang Z B, Tang W M and Lu Z H 2010 Effects of processing conditions on the work function and energy-level alignment of NiO thin films *J. Phys. Chem.* C. **114** 19777–81
[28] Sachtler W M H, Dorgelo G J H and Holscher A A 1966 The work function of gold *Surf. Sci.* **5** 221–9
[29] Nandy S, Maiti U N, Ghosh C K and Chattopadhyay K K 2009 Enhanced p-type conductivity and band gap narrowing in heavily Al doped NiO thin films deposited by RF magnetron sputtering *J. Phys. Condens. Matter* **21** 115804
[30] Dastan D *et al* 2023 Influence of heat treatment on H2S gas sensing features of NiO thin films deposited via thermal evaporation technique *Mater. Sci. Semicond. Process.* Elsevier Ltd **154** 107232
[31] Sarcan F, Aydin M, Kuruoğlu F, Donmez O, Yildirim S and Erol A 2021 Temperature-dependent sandwich and in-plane optical characterization of ternary chalcogenide TlSbS2 *Mater. Sci. Eng.* B **272** 115322
[32] Doğan Ü, Sarcan F, Koç K K, Kuruoğlu F and Erol A 2022 Effects of annealing temperature on a ZnO thin film-based ultraviolet photodetector *Phys. Scr.* **97** 15803
[33] Wang G *et al* 2024 Tunable contacts of Bi_2O_2Se nanosheets MSM photodetectors by metal-assisted transfer approach for self-powered near-infrared photodetection *Small* **20** 1–9
[34] Surender S *et al* 2023 Fabrication of composition-controlled MOCVD grown InxGa1-xN based MSM photodetectors *Opt. Mater. (Amst).* **136** 113462
[35] Dubey A *et al* 2020 Aluminum plasmonics enriched ultraviolet GaN photodetector with ultrahigh responsivity, detectivity, and broad bandwidth *Adv. Sci.* **7** 1–7
[36] Abadi A, Abubakr E, Oshita M, Noda D, Ohta R and Kan T 2024 Characterization of an uncooled mid-infrared Schottky photodetector based on a 2D Au/PtSi/p-Si nanohole array at a higher light modulation frequency *Appl. Opt.* **63** 2046–55
[37] Yoo T J *et al* 2021 A facile method for improving detectivity of graphene/p-type silicon heterojunction photodetector *Laser Photon. Rev.* **15** 2000557
[38] Boutwell R C, Wei M, Scheurer A, Mares J W and Schoenfeld W V 2012 Optical and structural properties of NiMgO thin films formed by sol–gel spin coating *Thin Solid Films* **520** 4302–4
[39] Guo Y M, Zhu L P, Jiang J, Hu L, Ye C L and Ye Z Z 2012 Valence band offset of n-ZnO/p-Mg x Ni1 − x O heterojunction measured by x-ray photoelectron spectroscopy *Appl. Phys. Lett.* **101** 52109